

<https://doi.org/10.1038/s41612-024-00588-3>

Contrasting sensitivity of air temperature trends to surface soil temperature trends between climate models and reanalyses



Yumeng Qiao¹, Guojie Wang², Daniel Fiifi Tawia Hagan^{1,3}✉, Kenny Thiam Choy Lim Kam Sian⁴,
Liangzhi Chen^{5,6}, Juha Aalto^{7,8}, Shijie Li¹, Xiao Zou¹ & Jiao Lu⁴

The sensitivity strength of air temperature (T) to surface soil temperature (sST) (namely β hereafter) constitutes a significant factor in how global climate models quantify changes in the climate. This study examines how this sensitivity is represented in the CMIP6 models. Results show regional differences and even contrasts in the β trends at interannual scales between climate models and two reanalysis products during 1980–2014. At high latitudes in the Northern Hemisphere (NH), β is stronger in the CMIP6 models than in the reanalysis data. Additionally, the β trends differ between the CMIP6 and reanalysis data, which may be related to the different precipitation (PR) and soil water availability (PR-ET) trends between the models. In the regions of increasing β intensity at high latitudes in the NH, sST is more sensitive to PR and PR-ET. Consequently, increasing PR and PR-ET leads to slower sST changes, potentially making β intensity stronger in CMIP6 models. However, in the reanalysis data, decreases in PR and PR-ET accelerate sST changes, leading to a weakening of the β intensity. A resulting implication is that β , based on high-emission scenarios, shows a stronger trend during 2015–2100, although this trend could potentially be overestimated. The findings contribute to a better understanding of the sensitivity of T to sST and facilitate the assessment of energy exchange between the land surface and the atmosphere in climate models.

The growing understanding of land-atmosphere interactions is driven by in-depth studies into land surface factors such as vegetation, soil moisture, surface soil temperature (sST), and snow cover (SND)^{1–7}. These studies have also shown that near-surface air temperature (T) and sST are fundamental variables that govern energy exchange between the land surface and the atmosphere and thus are critical in land-atmosphere interactions^{8,9}. On the one hand, alterations in global temperature and precipitation (PR) patterns lead to substantial changes in subsurface thermal conditions, subsequently influencing changes in sST¹⁰. On the other hand, changes in land surface factors could either further intensify or hamper T and PR trends¹¹.

The sensitivity of T to sST (β), described here as the regression slope between sST and T (simply sST- T coupling), quantifies how quickly T responds to changes in sST. The sST- T coupling is critical for the heat

balance between the Earth's land surface and the atmosphere, ecosystem respiration, and vegetation growth^{12–15}. Land-atmosphere coupling is not only an important indicator for assessing permafrost mapping and monitoring, agricultural production, ecological equilibrium, and thermodynamic processes within the climate system, but also involves multiple biophysical and biogeochemical processes^{16–22}. The variations in T directly reveal climate change trends, while sST represents the state of surface energy and heat transfer conditions^{23–25}. Through the surface energy balance and interactions within the climate system, sST influences T changes on both regional and global scales^{26–30}. Changes in sST can indirectly affect T , confounded by environmental factors such as solar radiation, soil thermal conductivity, and soil moisture content^{20,31–34}. For example, the growth of vegetation and its transpiration processes regulate sST by releasing

¹School of Geographical Sciences, Nanjing University of Information Science and Technology, Nanjing 210044, China. ²School of Remote Sensing and Geomatics Engineering, Nanjing University of Information Science and Technology, Nanjing 210044, China. ³Hydro-Climate Extremes Lab, Ghent University, Ghent 9000, Belgium. ⁴School of Atmospheric Science and Remote Sensing, Wuxi University, Wuxi 214105, China. ⁵Swiss Federal Institute for Forest, Snow and Landscape Research, Birmensdorf, Switzerland. ⁶Dynamic Macroecology, Swiss Federal Research Institute WSL, Birmensdorf, Switzerland. ⁷Weather and Climate Change Impact Research, Finnish Meteorological Institute, Helsinki, Finland. ⁸Department of Geosciences and Geography, University of Helsinki, Helsinki, Finland.

✉ e-mail: daniel.hagan@ugent.be

moisture, thereby influencing the surrounding $T^{45,36}$. Additionally, higher sST can increase evapotranspiration (ET), resulting in higher humidity levels that subsequently impact $T^{41,37}$. Soil water availability (PR-ET), including soil moisture, snow sublimation, ice coverage, and surface water, can also regulate the hydrothermal exchange between the atmosphere and the land surface²⁰.

Several studies have examined changes in β using temperature disparities, numerical models, and nonparametric methods to assess whether sST tracks changes in $T^{22,33,38}$. Evidence from local and regional studies strongly suggests that the relationship between sST and T is inconsistent over the long term and shows considerable difference between the two^{34,39–42}. For example, Fang et al.³⁸ and García-García et al.⁴³ highlight the temporal difference between sST and T changes. This difference is often influenced by various environmental changes, such as the retreat of glaciers and snow cover due to global warming, biomass loss, and worsening drought conditions^{11,44–48}. These factors can hinder or enhance the sST- T coupling.

Most studies that have assessed β are mainly based on historical observations, which are limited across space and time^{33,49}. Recent advances in data assimilation have provided a way to dynamically combine modeled data and observations, making reanalysis products more reliable⁵⁰. While all these datasets have been helpful in understanding historical β , some uncertainties persist concerning the impact of global warming on changes in β .

The Coupled Model Intercomparison Project (CMIP), initiated by the World Climate Research Program (WCRP), is currently in its sixth phase (CMIP6), consistently contributing to comprehensive scientific research on climate change and its impacts from the past into the future^{51,52}. CMIP6 models focus on earth system processes, and numerous studies have validated the reliability of model datasets at pixel or regional scales^{53–56}. While these datasets have demonstrated their relevance in projecting the potential impacts of global warming, certain uncertainties in the data have also been noted^{57,58}. Several evaluation studies have assessed the uncertainty of climate model data in various regions, using observational data, reanalysis data, and various validated datasets^{54,59,60}. For example, Zhao et al. and Dong et al.^{59,61} evaluated the uncertainties within the CMIP6 datasets using observational data, revealing internal inconsistencies within the models, especially with respect to ET. Such previous climate model assessments have guided the present study, which focuses on analyzing the impact of sST- T coupling differences within CMIP6 on β to better understand associated uncertainties in the prediction results.

The intensity of β , as a significant factor in quantifying climate change, primarily involves assessing the interannual relationship between sST and T . The strength of β may be influenced by other environmental variables such as seasonal SND, vegetation cover, and PR^{13,46,62}. While numerous studies have analyzed historical variations in β and the impact of environmental conditions using observational data, our focus is to explore how the CMIP6 datasets quantify this sensitivity and to understand the potential implications of reported deviations in other variables and climate processes on β . We first assessed the potential differences in interannual and seasonal differences between the climate models (CMIP6) and two reanalysis frameworks (the second Modern Research and Applications Retrospective Analysis (MERRA2) and the European Centre for Medium-Range Weather Forecasts (ECMWF) fifth generation reanalysis (ERA5) in the historical period 1980–2014. By analyzing factors influencing β in the two families of datasets, including trends and correlations of variables such as PR, PR-ET, SM, SND, and LAI (see Supplementary Table 1), we identified variables with contrasting trends in climate models compared to reanalysis datasets. Then, we investigated the evolution of β to the end of the 21st century under two projected warming scenarios (SSP1-2.6 and SSP5-8.5). This study aims to fill the gap in β research, focusing on sST at a soil depth of 0–0.05 m beneath the surface vegetation, and its variations between comparative model simulations and reanalysis data. Throughout the study, we conducted detailed data analysis to understand the differences between climate models and reanalysis datasets, focusing on factors that may influence changes in β intensity. This contributes to a more comprehensive understanding of the evolution of

key drivers of climate change and helps to predict and interpret future trends in climate change.

Results

Historical β variations and trends

To understand the spatiotemporal characteristics of historical β in the NH, we computed the mean and trends of the 16-year running window of 2-m sST (0–0.05 m beneath the surface vegetation) and T in the NH during 1980–2014 for CMIP6, MERRA2, and ERA5 (Fig. 1). For a more convenient analysis of the spatial distribution of β , we divided the NH latitudes into low-latitude (0°–30°N), mid-latitude (30°N–60°N) and high-latitude (above 60°N). The results show that the mean spatial distribution of β from the three datasets is relatively similar over the NH (Fig. 1a). β increases from north to south, indicating that long-term changes in T sensitivity to sST change are lower at high latitudes than at mid- and low latitudes. The lower sensitivity in the NH may be related to snow and freeze-thaw, where snow is an effective insulating layer and thus reduces sST variability⁶³. Due to the thermal inertia of the soil, moisture has a buffering effect by controlling thermal inertia³². The freeze-thaw cycle affects the state and distribution of moisture in the soil, resulting in frozen soil having a lower thermal conductivity than unfrozen soil^{64,65}. As a result, the transfer of heat from the atmosphere to the surface leads to relatively smaller changes in sST. These result in discrepancies between sST and T changes in high-latitude regions, resulting in lower sensitivity compared to low-latitude regions.

Compared with the reanalysis data (ERA5 and MERRA2), CMIP6 shows higher β at high latitudes. The spatial distributions of the sensitivity trends based on CMIP6, MERRA2, and ERA5 are shown in Fig. 1b for only statistically significant β ($p < 0.05$). However, sensitivity trends in the two reanalysis data show contrasting results at high latitudes in the NH compared to the CMIP6 models. The CMIP6 models show that the β trend increases from 1980 to 2014 in the northern Eurasian region, while the reanalysis data show a decreasing sensitivity. Meanwhile, over North America, we found decreases in the CMIP6 models and increases in the reanalysis. We note that the results of the reanalysis data are consistent with previous studies that also found a decreasing trend in β in northern Eurasia in recent decades based on observations⁸. However, the results indicate the contrary in some regions for the CMIP6 models β trends. These results suggest some discrepancy between the two families of datasets in the region.

Figure 1 represents the ensemble average results of the CMIP6 models. To better analyze the differences in β trends between different models, we calculated the spatial correlations between the β trends of 17 CMIP6 models during the historical period and the reanalysis data, as shown in Supplementary Table 2. The spatial correlations of β trends between the ACCESS-CM2, EC-Earth3, EC-Earth3-Veg-LR, and IPSL-CM6A-LR models with MERRA2 and ERA5 are positive, while the spatial correlations of the other models are negative, indicating a majority disagreement.

Next, we explored the β trends in detail by examining the seasonal changes. Figure 2 shows the interannual variations by seasons of β trends for the models and reanalysis data from 1980–2014. Here, we also found that the sensitivity strength of the three datasets varies with seasons and latitudes. In spring (MAM), β trend changes are smaller in CMIP6 than those in the reanalysis data. Nonetheless, β intensity of all three datasets shows an increasing trend in the low-latitude region of the NH. In the mid-latitude region, the reanalysis data show a noticeable decreasing sensitivity intensity trend, while there is little change in CMIP6. We find some differences in β trends at high latitudes. The CMIP6 β trends in the high-latitude region, such as the European region, increase, while the β trends in the reanalysis data decrease. All three datasets show an increasing trend in mid-latitudes, while CMIP6 sensitivity increases and MERRA2 and ERA5 sensitivity decreases in low-latitudes.

In summer (JJA), the difference in sensitivity intensity between datasets is significantly lower. The sensitivity of the three datasets increases to a lesser extent in high latitudes, decreases in mid-latitudes, and increases in low latitudes. Figure 2 shows similar β trends in autumn (SON) patterns to that in MAM in the NH high-latitude regions. In autumn, the β trend of CMIP6 is

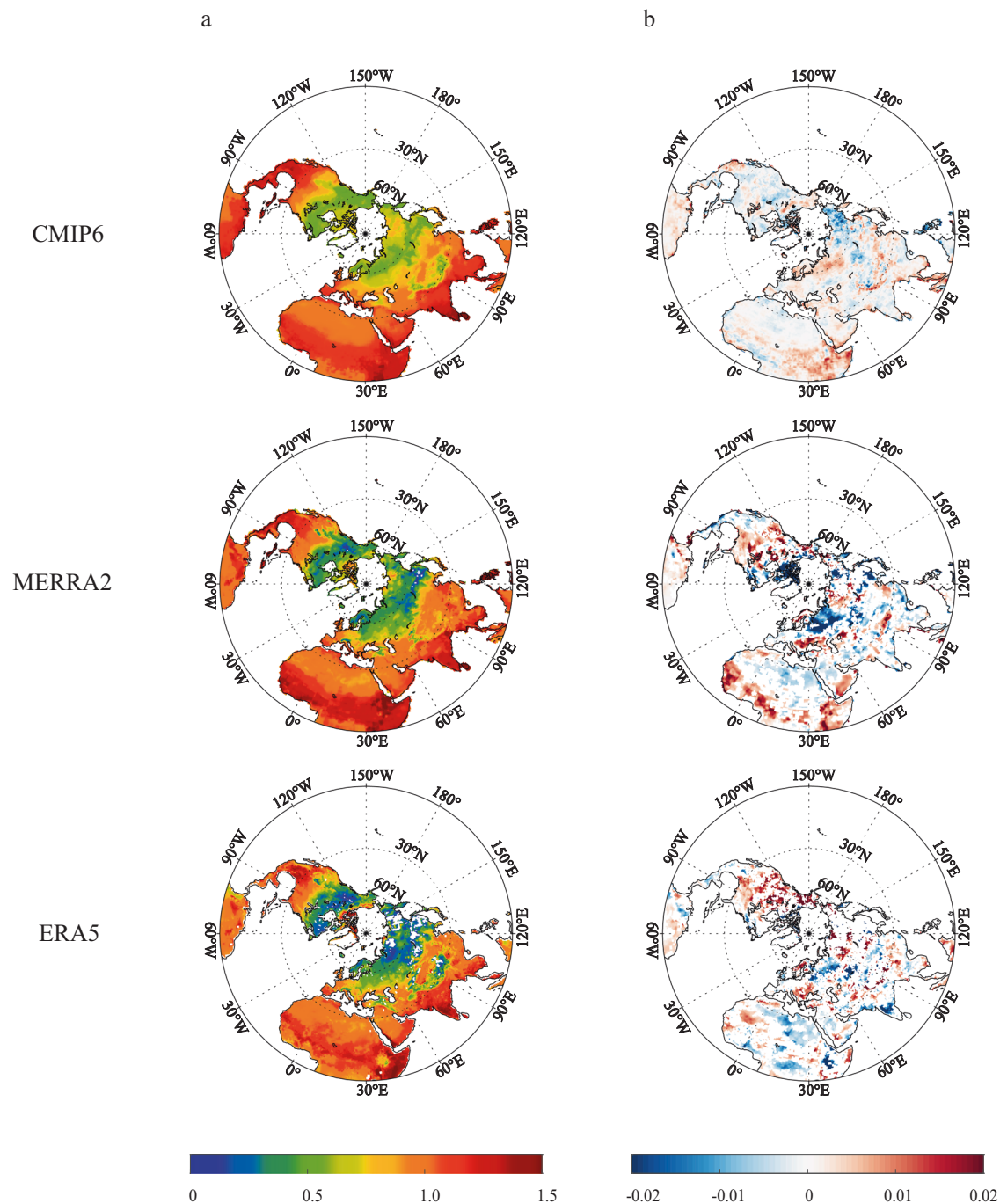


Fig. 1 | Spatial distribution of sensitivity of T to sST (β) and trend in the NH from CMIP6, MERRA2, and ERA5 during 1980–2014. a Annual mean of β . b β trend with a 16-year sliding window. β trends are significant at $p < 0.05$. The figure shows only statistically significant pixels, while white pixels indicate no statistical significance.

weaker compared to the reanalysis data. At high latitudes, especially in the European region, CMIP6 shows an increasing β trend while that of the reanalysis data decreases. The sensitivity trends are more consistent in the low and middle latitudes. However, some differences are noticeable in the lower latitudes towards the tropical regions. We also found some contrasting trends even between the reanalysis products in SON along the Sahelian region, which is explored later in this paper. The overall spatial distribution of the seasonal sensitivity trends during the thawing (spring, MAM) and freezing period (autumn, SON) is consistent with the annual average.

β of the three datasets at low- and mid-latitudes in the NH shows a decreasing trend in winter, and CMIP6 still shows an increasing trend in the European region at high latitudes. In contrast, a decreasing trend is observed in MERRA2, while no significant change is noted in the sensitivity strength

of ERA5. The presence or absence of snow significantly affects shallow SST in areas with seasonal snowfall⁶². The thickness of snow directly affects the energy transfer between the near-surface and the atmosphere. Seasonal snow acts as an effective obstacle that separates shallow soil layers from immediate local meteorological conditions⁶⁶. The early disappearance of the spring snowpack, the shorter duration of the seasonal snowpack, and the reduction in snow thickness all lead to a weaker snowpack insulating effect on sST , resulting in a decreasing sensitivity trend in spring in the high-latitude snowpack regions.

To further investigate the reasons for the β trends differences, we intercompared the temporal difference of the spatial average of positive β trends in CMIP6 with corresponding pixels in MERRA2 and ERA5, as well as regions of negative trends as shown in Fig. 3. Here, we obtained the

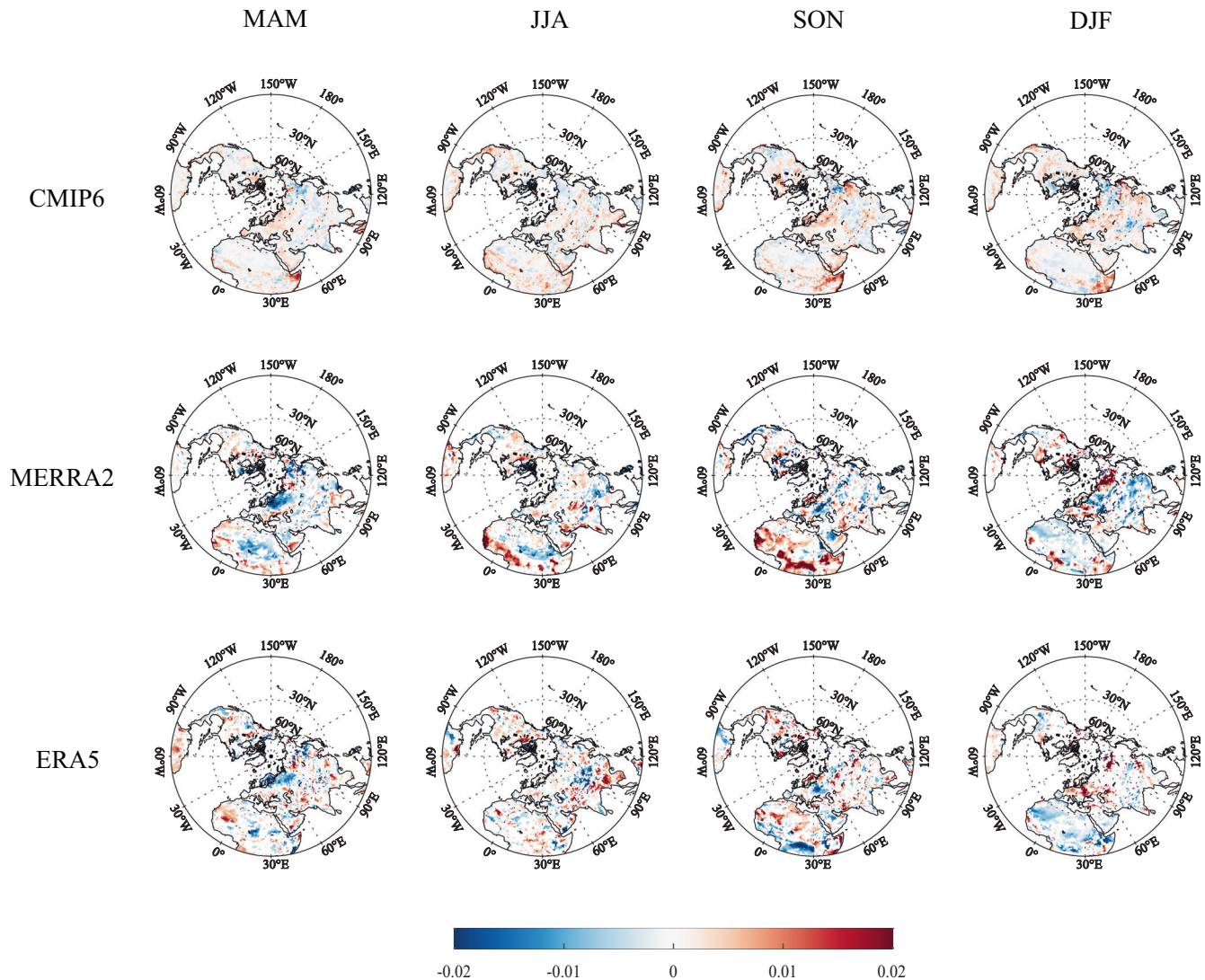


Fig. 2 | β trend of CMIP6, MERRA2, and ERA5 in different seasons from 1980 to 2014. Spring (MAM); summer (JJA); autumn (SON); winter (DJF). The β trends are significant at $p < 0.05$. The figure shows only statistically significant pixels, while white pixels indicate no statistical significance.

temporal variations by computing 16-year running window β variations from 1980 to 2014. Figure 3a shows that the regions of negative β trends in CMIP6 are consistent with the reanalysis datasets. The results also demonstrate that the decreasing trends are mainly determined by the temporal variation of β after 2005 in both model families. On the other hand, the regions (Fig. 3b) of positive β trends in CMIP6 appear to be consistent in the temporal variations before 2005. However, the two model families contrast in their temporal trends from 2005 to 2014. After 2005, the β of the two reanalysis data decreases, but the sensitivity intensity of CMIP6 data still increases. Thus, we deduced here that the differences in sensitivity strengths mainly occur in regions with increasing CMIP6 sensitivity strength, i.e., low-latitude and European regions, as shown in Fig. 1. Considering the sensitivity trends at these time scales, we found that β trend differences are particularly pronounced in the European region, where previous studies have shown that the sST-T coupling decreases over time in northern Eurasia. This decrease is associated with higher temperatures and reduced snow area during snow-free periods, consistent with the results from the reanalysis data⁸.

Possible mechanisms influencing β trends

Several factors could account for the contrasting trends in the two model families. Here, we computed the slopes (k) and correlations (R^2) of PR, PR-

ET, SM, SND, and LAI (see Supplementary Table 1) to consider the influencing factors of β comprehensively. Comparing these variables shows that both SM and SND exhibit a decreasing trend across climate models and reanalysis data, while LAI shows no interannual variation in the reanalysis data, making it unnecessary for further analysis. However, PR and PR-ET show divergent trends between CMIP6 models and reanalysis data, with an increasing trend in CMIP6 and a decreasing trend in the reanalysis data. Given the discrepancy in trends for PR and PR-ET within these model families, we selected these two variables for further analysis to explore the different trends of β within the models. Figure 4 shows the interannual trends in PR and PR-ET in the NH and the temporal variation of CMIP6, MERRA2, and ERA5 PR and PR-ET in areas where the sensitivity strength of CMIP6 is increasing. The reanalysis data shows a decreasing β in the region, contrasting with the increasing β in CMIP6. Factors affecting β differences between CMIP6 and reanalysis data vary at different spatial and temporal scales. Here, we analyzed the trends and temporal changes of PR and PR-ET to infer its potential relation with β trends for the entire period for the NH (Fig. 4). Figure 4a shows consistently positive PR trends in most parts of the NH in the CMIP6 models, especially across the Eurasian region and northern Africa. On the other hand, the reanalysis models show strongly negative trends in these regions. Similarly, the trend of PR-ET increases in most of the NH in the CMIP6 models; however, the opposite

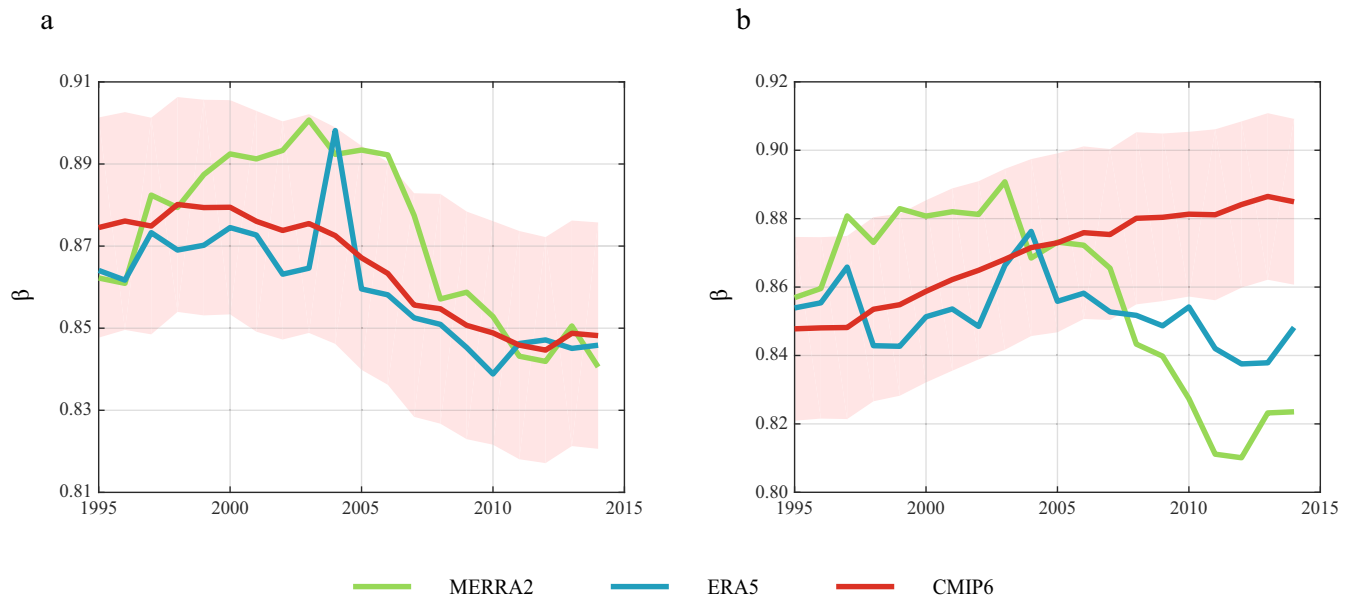


Fig. 3 | Temporal variation of β in CMIP6, MERRA2, and ERA5 from 1980 to 2014. Spatially averaged temporal variation of β for **a** regions of negative β trends in the multi-model mean and **b** regions of positive β trends in the multi-model mean using a 16-year running window. The red, green, and blue lines are the CMIP6,

MERRA2, and ERA5 results, respectively. x axis is the time beginning with the last year of the first 16-year running window (e.g., 2005 indicates the running window from 1990 to 2005). y axis indicates the sensitivity strength. The red shading indicates the standard deviation interval of the 17 CMIP6 models' sensitivity.

trend is observed in the reanalysis data (Fig. 4b). It is worth noting that there is a significant difference between the models and reanalysis data with opposite PR trends (Fig. 4c) in the areas where β in the CMIP6 models increases. Furthermore, the temporal variation of PR-ET, although smaller than that of PR, has the opposite PR-ET trends between models and reanalysis data (Fig. 4d). In the region where the CMIP6 sensitivity is rising, the CMIP6 PR and PR-ET show an increasing trend, while that of the reanalysis data show a decreasing trend.

To further investigate the key mechanisms affecting the differences in β trends between climate models and reanalysis data, we computed the sensitivity of PR to sST and T and PR-ET to sST and T . First, we determined the sensitivities of PR and PR-ET to sST and T , respectively. Figure 5a represents the spatial averaging of the sensitivity of PR and PR-ET to sST in the region of increasing β trends in CMIP6. At the same time, Fig. 5b shows the spatial averaging of the sensitivity of PR and PR-ET to T in the region of increasing β trends in CMIP6. The results show that the sensitivity of both PR and PR-ET to sST and T tends to decrease in the region of increasing CMIP6 β trend, especially after 2005 when CMIP6 decreases significantly, while reanalysis data show no significant change. Then, to compare the sensitivity of PR to sST and T (PR-sST and PR- T) and PR-ET to sST and T (PR-ET-sST and PR-ET- T) between the climate models and reanalysis data, we subtracted PR- T from PR-sST and PR-ET- T from PR-ET-sST and calculated the spatial average of the regions of increasing β trends in CMIP6 (Fig. 5c). A positive value indicates a higher sensitivity of PR or PR-ET to sST, while a negative value indicates a higher sensitivity of PR or PR-ET to T . Combining Supplementary Fig. 2 and Fig. 3, in the region of increasing CMIP6 β during 2005–2014, PR and PR-ET show increasing sensitivity to sST in the CMIP6 models, while there is a slight weakening trend in the reanalyses. This suggests that during this period, the influence of PR and PR-ET on β in the CMIP6 models gradually shifts from controlling T changes to controlling sST changes. In the CMIP6 models, the increase in PR and PR-ET leads to the evaporation of SM, which absorbs a considerable amount of heat from the environment and consequently slows down the sST changes. In the reanalysis data, however, the decrease in PR and PR-ET leads to soil drying and reduced evaporation. This directs energy primarily to land surface heating, accelerating sST changes and weakening β intensity. These trends help explain the differences in β trends between climate models and reanalysis data from 2005 to 2014, as shown in Fig. 3b. Regions across the

Sahelian belt of Africa also show this pattern even more strongly. These results are consistent with the findings in Fig. 4, where PR and PR-ET trends are opposite between CMIP6 and the reanalysis models. Thus, we suggest that the differences in how PR and PR-ET trends are represented in the models are a potentially viable reason for the contrasting sST- T sensitivity trends.

Future β trends

Figure 6 shows β trends for two future scenarios in the CMIP6 climate models (2015–2100): a sustainable world of low emissions (Shared Socio-economic Pathways, SSP1-2.6) and a fossil fuel-driven world of high emissions (SSP5-8.5) (Fig. 6). In this section, we also averaged the models with historically positive spatial correlations (HPSC) and historically negative spatial correlations (HNSC) with the MERRA2 and ERA5. Firstly, the results from the average of all the CMIP6 models and the average of the models with HPSC show that the regions and magnitudes of positive β trends in SSP5-8.5 (Fig. 6d, e) are more pronounced compared to the β trend changes in SSP1-2.6 (Fig. 6a, b). This shows that β trends increase with increasing emission scenarios, both in the total average and in the HPSC model average (Fig. 6a, b, d, e). Figure 6b, e shows that in the low-latitude regions of the NH, β trends show a negative trend, while in the mid-to-high-latitude regions, β trends increase. This pattern is stronger with increasing emission scenarios as well. To understand the potential bias in the future β trends of the CMIP6 models, we computed the difference between the HPSC and HNSC (HPSC-HNSC) as shown in Fig. 6c, f. Here, the HPSC average is used as a relative baseline since it is assumed to be closer to the truth. In the SSP1-2.6 scenario (Fig. 6c), the HPSC shows a pronounced increase in β trends in the mid-to-high-latitude regions of the NH. However, in the SSP5-8.5 scenario (Fig. 6f), HNSC overestimates the β trends for the future period. These results show that T becomes more sensitive to sST under the high-emission scenario. This bias is indicated by a higher increase in β trends in the HNSC models, which would contribute to increasing T trends as expected in SSP5-8.5.

Discussion

β distribution appears to be more consistent at low and mid-latitudes, in the NH, in all the models within the study period, showing that T is more strongly coupled with sST in these regions (Supplementary Fig. 1). In

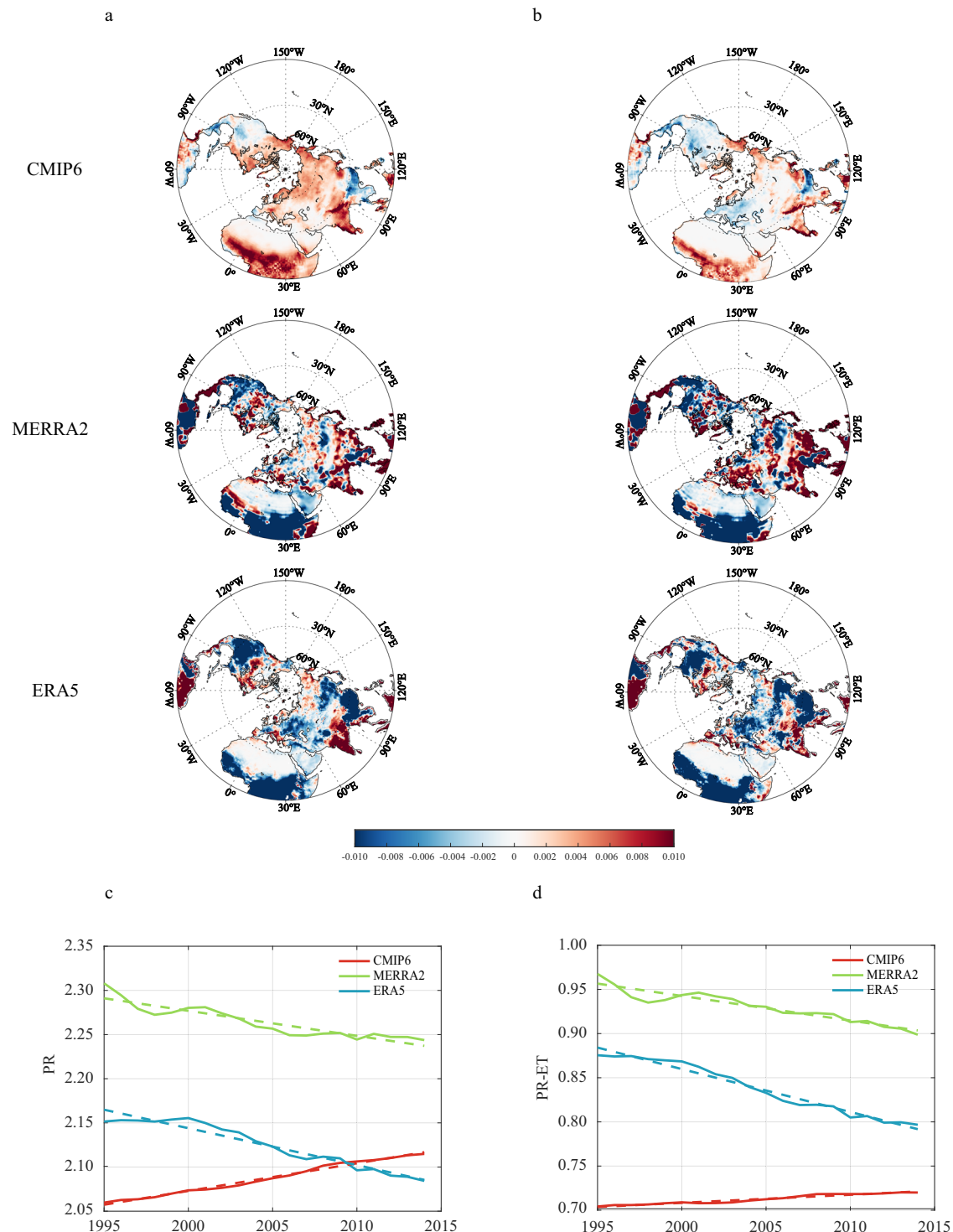


Fig. 4 | Spatiotemporal variation of precipitation (PR) and soil water availability (PR-ET) in CMIP6, MERRA2, and ERA5 during 1980–2014. Spatial distribution of trends in **a** PR and **b** PR-ET, and temporal changes in **c** PR and **d** PR-ET calculated for CMIP6 (red line), MERRA2 (green line), and ERA5 (blue line) based on the

CMIP6 β positive region. The x axis represents the last year of each 16-year running window, and the y axis represents the influencing factors (units: mm month⁻¹). The dashed line indicates the fitted line.

general, β is influenced by various environmental factors, and its intensity varies with latitude. The results show that β and its trends in the NH high latitudes from 1980–2014 are inconsistent between climate models and reanalysis data, which are related to the differences in PR and PR-ET trends.

Further seasonal analysis reveals that disparities in sensitivity trends between climate models and reanalysis data primarily manifest during the freeze-thaw period, attributed to the insulating effect of snow and the impact

of permafrost on sST, resulting in nonconformity between sST and T changes in high-latitude regions^{6,67}. Comparing CMIP6 with the reanalysis data during the thawing and freezing periods, the results of the sensitivity trend are also contrasting, indicating that CMIP6 does not better reflect the changes in β . Due to the seasonal differences in the region, it could be inferred that the differences in sensitivity may be related to the influence of seasonal snowfall and freezing on sST in the models. Frozen PR is stored in

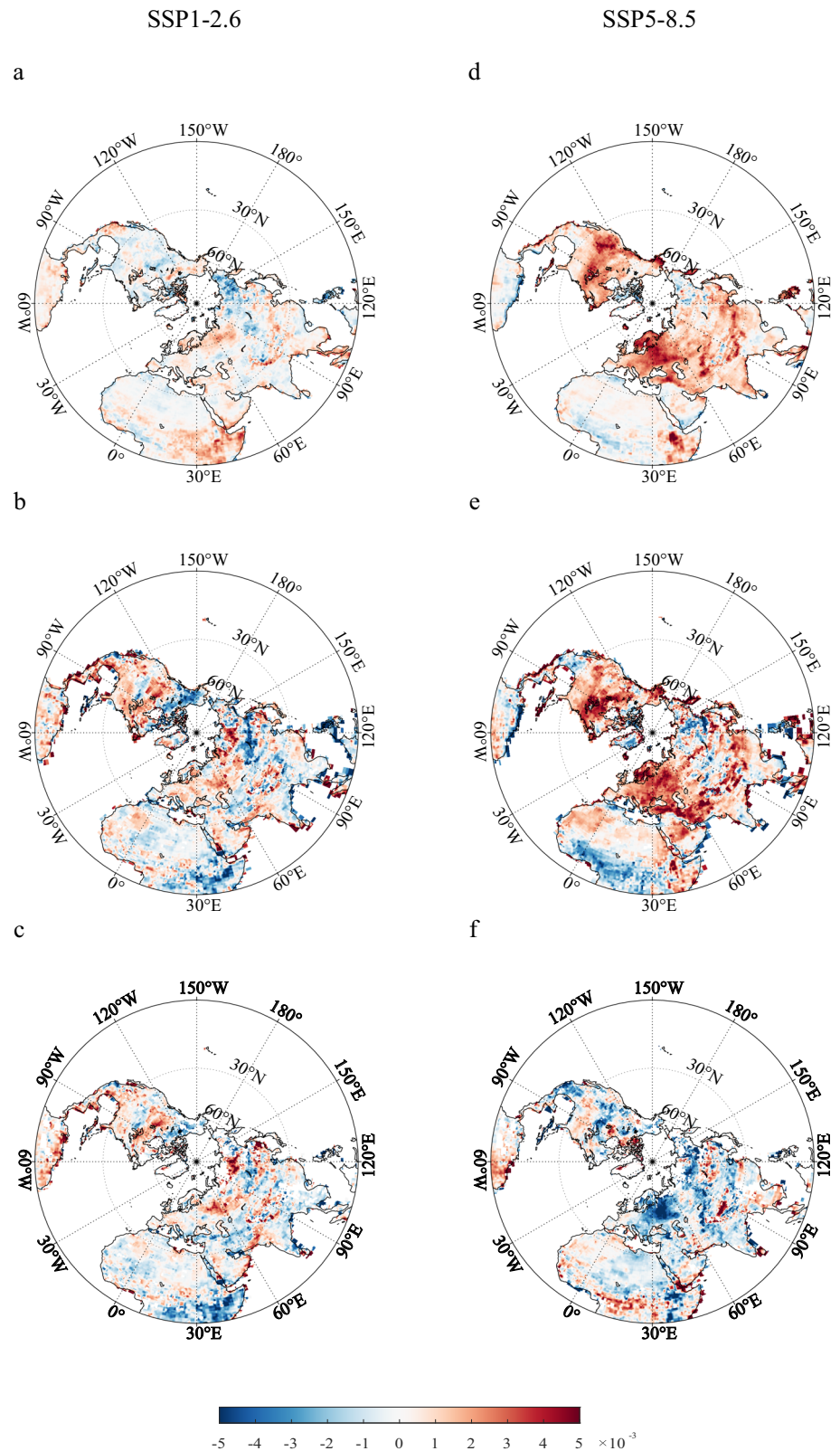


Fig. 5 | Temporal variation of PR and PR-ET sensitivity to sST and T in CMIP6, MERRA2, and ERA5 during 1980–2014. Spatially averaged **a** PR and PR-ET sensitivity to sST, **b** PR and PR-ET sensitivity to T, and **c** PR and PR-ET sensitivity differences to sST and T for CMIP6 (red line), MERRA2 (green line), and ERA5 (blue line) in the CMIP6 β positive region.

the snowpack from autumn to spring, changing the surface albedo and affecting the radiation and energy fluxes at the land-atmosphere interface. In spring, freshwater released from snowmelt contributes to soil infiltration and directly regulates surface ET⁶⁸. The overall spatial distribution is

consistent with the annual average sensitivity trend, with the model sensitivity showing an increasing trend in most areas at high latitudes and a significant decreasing trend in the reanalysis data. In contrast, a possible reason for the relatively insignificant differences in sensitivity trends during

Fig. 6 | Spatial distribution of β trends from 2015 to 2100. β trends for the a–c SSP1-2.6 and d–f SSP5-8.5 for CMIP6. **a, d** Average β trends across 17 models. **b, e** Average β trends from models with historically positive spatial correlations with reanalysis data. **c, f** The difference between the average β trends from models with historically positive spatial correlations with reanalysis data and the average from models with historically negative spatial correlations. The figure shows only statistically significant pixels at $p < 0.05$, while white pixels indicate no statistical significance.



the summer could be the frequent PR, which increases surface humidity, leading to increased evaporation demand and lower land temperatures and ultimately contributing to a relatively slower rate of sST change^{33,40}. The interannual variation of sST with respect to T is greater when there is snow on the land than when there is no snow in summer, indicating that the change in sST in winter is not necessarily proportional to the change in T .

Thus, CMIP6, MERRA2, and ERA5 data can show inconsistent changes in sensitivity strength in high-latitude snow or permafrost regions.

sST is a valuable parameter for monitoring climate change as it integrates most processes occurring at and above the Earth's surface, including T , PR, snowfall, and vegetation. This study suggests that investigating whether changes in sST within the CMIP6 models follow T variations

contributes to understanding the potential shifts in future climate. Prior research has found that some CMIP6 models simulate more intense warming, leading to overestimating warming trends⁶⁹. Coupled with increasing sensitivity trends in climate models, this could potentially lead to an overestimation of sensitivity intensity in future periods.

The sensitivity of T to deep soil temperature is not considered in this study since only soil depths in the range of 0–0.05 m are used. This may neglect the time lag between sST and T , which may then affect β . Also, the least squares regression for calculating the sensitivity only considers the positive values and does not analyze the areas where the sensitivity is negative. The physical mechanisms of sST and T and the changes in the sensitivity trend between sST and T at different depths need to be further explored in future work. We analyzed the trends and R^2 values related to PR, PR-ET, SM, SND, and LAI (see Supplementary Table 1). Although we selected PR and PR-ET as the primary variables influencing the β trend, when evaluating the correlation between these variables and β , we found that SM and SND also play roles in altering β . This might be due to our use of monthly data, which may not adequately capture the influence of SM and SND on β trends at lower temporal resolutions. However, these effects may be more pronounced at higher temporal scales.

Methods

Datasets

In this study, the β for historical (1980–2014) and future (2015–2100) periods is obtained from CMIP6 models. We considered two future scenarios of economic and human development (SSP1-2.6 and SSP5-8.5). Other variables that were considered are monthly 2-m T , shallow sST, PR, and ET. Monthly sST and T data were averaged as annual and seasonal values, and monthly PR and ET was averaged as annual values. In the CMIP6 climate models, sST from 0–0.05 m depth is selected. In addition, to ensure model performance, provide scientific reference for climate change, and facilitate analysis and comparison, the model was unified onto a $0.5^\circ \times 0.5^\circ$ grid, and we focused on the sensitivity analysis of the multi-model average of the 17 CMIP6 models considered. Supplementary Table 3 lists the CMIP6 GCMs used in the study. All the models used the first variation member (r1i1p1f1) except for GISS-E2-1-G and UKESM1-0-LL, which use a forcing index of 2.

This study used two reanalysis datasets to validate the sensitivity calculated from CMIP6 data during the historical period. The significance of reanalysis datasets in climate monitoring applications has gained widespread recognition, and consequently, these datasets are extensively employed in climate studies. MERRA2 is a National Aeronautics and Space Administration (NASA) atmospheric reanalysis from 1980 with a spatial resolution of $0.5^\circ \times 0.625^\circ$ (lon×lat). Compared to MERRA1, MERRA2 has reduced some of the spurious trends and discrepancies associated with changes in the observations⁷⁰. ERA5 is a dataset generated using models and assimilation of various observations from around the globe, and has a much higher spatial resolution. Like MERRA2, it has been shown in previous studies to have a better representation of the spatial distribution of meteorological elements and changes in trends, with a spatial resolution of $0.25^\circ \times 0.25^\circ$ (lon×lat)⁷¹. For the comparative analysis of CMIP6 and reanalysis data, the spatial resolution of the data was standardized to $0.5^\circ \times 0.5^\circ$ (lon×lat) in this study.

Ordinary least squares regression

Currently, many research efforts used ordinary least squares regression to quantify the soil-atmosphere thermal coupling^{8,22}. Following Chen et al.⁸, β is calculated as the slope of the least squares regression between sST and T , representing sensitivity intensity¹⁹. The sensitivity value is in the range of 0 to 1.5, with higher values indicating stronger sensitivity. β quantitatively represents the responsiveness of T to changes in sST, and its intensity varies with soil depths²⁶. Our primary focus is to examine the interannual relationship between variations in these two elements.

Assuming that the equation for fitting a straight line is:

$$y = \beta \cdot x + b \quad (1)$$

where the slope of the fitted straight line is:

$$\beta = \frac{\overline{xy} - \bar{x} \cdot \bar{y}}{x^2 - (\bar{x})^2} \quad (2)$$

where x indicates sST and y indicates T . We calculated a 16-year running window for each grid point during the historical and future periods, using linear trends in β for the running windows (20 windows in total) to examine interannual variation in sensitivity. The fluctuations in the data are analyzed by removing the linear trend in each window before computing β , and removing the variation in the data caused by factors such as seasons.

To investigate the β change and the factors influencing the difference in β trend between the climate models and reanalysis data, we divided the sensitivity trend of CMIP6 into regions of increasing and decreasing sensitivity trends. We also computed the corresponding trends in the PR and PR-ET datasets, along with computing the sensitivity to changes in these variables. Through surface water balance relationships, we approximated the amount of available water by the difference between PR and ET⁷². A positive sensitivity indicates that PR is more sensitive to sST, and a negative sensitivity indicates that PR is more sensitive to T . Thus, we compared the β of the CMIP6 models with ERA5 and MERRA2, and analyze the reasons for the differences in sensitivity changes.

Data availability

Climate model data is available from the CMIP6 official website: <https://esgf-node.llnl.gov/projects/cmip6/>. MERRA2-Reanalysis data can be downloaded from the following website: <https://disc.gsfc.nasa.gov/datasets/project=MERRA-2>. ERA5-Reanalysis data can be downloaded from the following website: <https://cds.climate.copernicus.eu/cdsapp#!/search?type=dataset>.

Code availability

The codes used in this study can be obtained from the corresponding author upon request.

Received: 17 September 2023; Accepted: 2 February 2024;

Published online: 17 February 2024

References

- Li, Z. et al. A comprehensive review on coupled processes and mechanisms of soil-vegetation-hydrology, and recent research advances. *Sci. China Earth Sci.* **65**, 2083–2114 (2022).
- Zhao, C., Chen, H. & Sun, S. Evaluating the capabilities of soil enthalpy, soil moisture and soil temperature in predicting seasonal precipitation. *Adv. Atmos. Sci.* **35**, 445–456 (2018).
- Deng, Y. et al. Variation trend of global soil moisture and its cause analysis. *Ecol. Indic.* **110**, 105939 (2020).
- Helama, S., Tuomenvirta, H. & Venäläinen, A. Boreal and subarctic soils under climate change. *Glob. Planet. Change* **79**, 37–47 (2011).
- Seneviratne, S. I., Lüthi, D., Litschi, M. & Schär, C. Land-atmosphere coupling and climate change in Europe. *Nature* **443**, 205–209 (2006).
- Zhang, J., Wu, L. & Dong, W. Land-atmosphere coupling and summer climate variability over East Asia. *J. Geophys. Res. Atmos.* **116**, 1–14 (2011).
- Mackiewicz, M. C. A new approach to quantifying soil temperature responses to changing air temperature and snow cover. *Polar Sci.* **6**, 226–236 (2012).
- Chen, L., Aalto, J. & Luoto, M. Observed decrease in soil and atmosphere temperature coupling in recent decades over northern Eurasia. *Geophys. Res. Lett.* **48**, e2021GL092500 (2021).

9. Shati, F., Prakash, S., Norouzi, H. & Blake, R. Assessment of differences between near-surface air and soil temperatures for reliable detection of high-latitude freeze and thaw states. *Cold Reg. Sci. Technol.* **145**, 86–92 (2018).
10. Kurylyk, B. L., MacQuarrie, K. T. & McKenzie, J. M. Climate change impacts on groundwater and soil temperatures in cold and temperate regions: implications, mathematical theory, and emerging simulation tools. *Earth-Sci. Rev.* **138**, 313–334 (2014).
11. Wu, L. & Zhang, J. Strong subsurface soil temperature feedbacks on summer climate variability over the arid/semi-arid regions of East Asia. *Atmos. Sci. Lett.* **15**, 307–313 (2014).
12. Jiang, K. et al. Influence patterns of soil moisture change on surface-air temperature difference under different climatic background. *Sci. Total Environ.* **822**, 153607 (2022).
13. Bond-Lamberty, B. & Thomson, A. Temperature-associated increases in the global soil respiration record. *Nature* **464**, 579–582 (2010).
14. Liang, L., Riveros-Iregui, D., Emanuel, R. & McGlynn, B. A simple framework to estimate distributed soil temperature from discrete air temperature measurements in data-scarce regions. *J. Geophys. Res. Atmos.* **119**, 407–417 (2014).
15. Piao, S. et al. Forest annual carbon cost: a global-scale analysis of autotrophic respiration. *Ecology* **91**, 652–661 (2010).
16. Koven, C. D., Riley, W. J. & Stern, A. Analysis of permafrost thermal dynamics and response to climate change in the CMIP5 Earth System Models. *J. Clim.* **26**, 1877–1900 (2013).
17. Lesk, C. et al. Stronger temperature-moisture couplings exacerbate the impact of climate warming on global crop yields. *Nat. Food* **2**, 683–691 (2021).
18. Porter, J. R. & Gawith, M. Temperatures and the growth and development of wheat: a review. *Eur. J. Agron.* **10**, 23–36 (1999).
19. Lenoir, J., Hattab, T. & Pierre, G. Climatic microrefugia under anthropogenic climate change: implications for species redistribution. *Ecography* **40**, 253–266 (2017).
20. Seneviratne, S. I. et al. Investigating soil moisture-climate interactions in a changing climate: a review. *Earth-Sci. Rev.* **99**, 125–161 (2010).
21. Miralles, D. G., Van Den Berg, M., Teuling, A. & De Jeu, R. Soil moisture-temperature coupling: a multiscale observational analysis. *Geophys. Res. Lett.* **39**, 1–6 (2012).
22. Aalto, J., Scherrer, D., Lenoir, J., Guisan, A. & Luoto, M. Biogeophysical controls on soil-atmosphere thermal differences: implications on warming Arctic ecosystems. *Environ. Res. Lett.* **13**, 074003 (2018).
23. Chapin, F. S. III et al. Role of land-surface changes in Arctic summer warming. *Science* **310**, 657–660 (2005).
24. Zeng, L. et al. Estimation of daily air temperature based on MODIS land surface temperature products over the corn belt in the US. *Remote Sens.* **7**, 951–970 (2015).
25. García-Suárez, A. & Butler, C. Soil temperatures at Armagh observatory, Northern Ireland, from 1904 to 2002. *Int. J. Climatol.* **26**, 1075–1089 (2006).
26. Zhang, H., Yuan, N., Ma, Z. & Huang, Y. Understanding the soil temperature variability at different depths: effects of surface air temperature, snow cover, and the soil memory. *Adv. Atmos. Sci.* **38**, 493–503 (2021).
27. Qian, B., Gregorich, E. G., Gameda, S., Hopkins, D. W. & Wang, X. L. Observed soil temperature trends associated with climate change in Canada. *J. Geophys. Res. Atmos.* **116** (2011).
28. Xue, Y., Vasic, R., Janjic, Z., Liu, Y. & Chu, P. C. The impact of spring subsurface soil temperature anomaly in the western US on North American summer precipitation: a case study using regional climate model downscaling. *J. Geophys. Res. Atmos.* **117**, 1–11 (2012).
29. Yang, K. & Zhang, J. Spatiotemporal characteristics of soil temperature memory in China from observation. *Theor. Appl. Clim.* **126**, 739–749 (2016).
30. Liu, J., Hagan, D. F. T. & Liu, Y. Global land surface temperature change (2003–2017) and its relationship with climate drivers: AIRS, MODIS, and ERA5-land based analysis. *Remote Sens.* **13**, 44 (2020).
31. Chen, X. et al. The spatiotemporal variations of soil water content and soil temperature and the influences of precipitation and air temperature at the daily, monthly, and annual timescales in China. *Theor. Appl. Clim.* **140**, 429–451 (2020).
32. Cheruy, F., Dufresne, J.-L., Ait Mesbah, S., Grandpeix, J. & Wang, F. Role of soil thermal inertia in surface temperature and soil moisture-temperature feedback. *J. Adv. Model. Earth Syst.* **9**, 2906–2919 (2017).
33. Beltrami, H. & Kellman, L. An examination of short-and long-term air-ground temperature coupling. *Glob. Planet. Change* **38**, 291–303 (2003).
34. Zhan, M.-j, Xia, L., Zhan, L. & Wang, Y. Recognition of changes in air and soil temperatures at a station typical of China's subtropical monsoon region (1961–2018). *Adv. Meteorol.* **2019**, 1–9 (2019).
35. Foley, J. A., Kutzbach, J. E., Coe, M. T. & Levis, S. Feedbacks between climate and boreal forests during the Holocene epoch. *Nature* **371**, 52–54 (1994).
36. Chae, Y., Kang, S. M., Jeong, S. J., Kim, B. & Frierson, D. M. Arctic greening can cause earlier seasonality of Arctic amplification. *Geophys. Res. Lett.* **42**, 536–541 (2015).
37. Li, K., Zhang, J., Wu, L., Yang, K. & Li, S. The role of soil temperature feedbacks for summer air temperature variability under climate change over East Asia. *Earth's Future* **10**, e2021EF002377 (2022).
38. Fang, X., Luo, S. & Lyu, S. Observed soil temperature trends associated with climate change in the Tibetan Plateau, 1960–2014. *Theor. Appl. Clim.* **135**, 169–181 (2019).
39. Smerdon, J. E. et al. Daily, seasonal, and annual relationships between air and subsurface temperatures. *J. Geophys. Res. Atmos.* **111**, 1–12 (2006).
40. Zhang, Y., Chen, W., Smith, S. L., Riseborough, D. W. & Cihlar, J. Soil temperature in Canada during the twentieth century: Complex responses to atmospheric climate change. *J. Geophys. Res. Atmos.* **110**, 1–15 (2005).
41. González-Rouco, F., Von Storch, H. & Zorita, E. Deep soil temperature as proxy for surface air-temperature in a coupled model simulation of the last thousand years. *Geophys. Res. Lett.* **30**, 1–4 (2003).
42. García-García, A. et al. Soil heat extremes can outpace air temperature extremes. *Nat. Clim. Change* **13**, 1237–1241 (2023).
43. García-García, A., Cuesta-Valero, F. J., Beltrami, H. & Smerdon, J. E. Characterization of air and ground temperature relationships within the CMIP5 historical and future climate simulations. *J. Geophys. Res. Atmos.* **124**, 3903–3929 (2019).
44. Broxton, P. D., Zeng, X. & Dawson, N. The impact of a low bias in snow water equivalent initialization on CFS seasonal forecasts. *J. Clim.* **30**, 8657–8671 (2017).
45. Grundstein, A., Todhunter, P. & Mote, T. Snowpack control over the thermal offset of air and soil temperatures in eastern North Dakota. *Geophys. Res. Lett.* **32**, 1–4 (2005).
46. Genxu, W., Guangsheng, L., Chunjie, L. & Yan, Y. The variability of soil thermal and hydrological dynamics with vegetation cover in a permafrost region. *Agric. Meteorol.* **162**, 44–57 (2012).
47. Fischer, E. M., Seneviratne, S. I., Lüthi, D. & Schär, C. Contribution of land-atmosphere coupling to recent European summer heat waves. *Geophys. Res. Lett.* **34**, 1–6 (2007).
48. Winckler, J. et al. Different response of surface temperature and air temperature to deforestation in climate models. *Earth Syst. Dyn.* **10**, 473–484 (2019).
49. Schmidt, W. L., Gosnold, W. D. & Enz, J. W. A decade of air-ground temperature exchange from Fargo, North Dakota. *Glob. Planet. Change* **29**, 311–325 (2001).
50. Hagan, D. F., Wang, G., Parinussa, R. & Shi, X. Inter-comparing and improving land surface temperature estimates from passive

- microwaves over the Jiangsu province of the People's Republic of China. *Int. J. Remote Sens.* **40**, 5563–5584 (2019).
51. Zhang, S. et al. Coupled data assimilation and parameter estimation in coupled ocean–atmosphere models: a review. *Clim. Dyn.* **54**, 5127–5144 (2020).
 52. Eyring, V. et al. Overview of the coupled model intercomparison project phase 6 (CMIP6) experimental design and organization. *Geosci. Model Dev.* **9**, 1937–1958 (2016).
 53. Kamruzzaman, M. et al. Comparison of CMIP6 and CMIP5 model performance in simulating historical precipitation and temperature in Bangladesh: a preliminary study. *Theor. Appl. Clim.* **145**, 1385–1406 (2021).
 54. Yang, X., Zhou, B., Xu, Y. & Han, Z. CMIP6 evaluation and projection of temperature and precipitation over China. *Adv. Atmos. Sci.* **38**, 781–830 (2021).
 55. Li, J. et al. Evaluation of CMIP6 global climate models for simulating land surface energy and water fluxes during 1979–2014. *J. Adv. Model. Earth Syst.* **13**, e2021MS002515 (2021).
 56. Tian-Jun, Z., Li-Wei, Z. & Xiao-Long, C. Commentary on the coupled model intercomparison project phase 6 (CMIP6). *Adv. Clim. Change Res.* **15**, 445 (2019).
 57. Taylor, K. E., Stouffer, R. J. & Meehl, G. A. An overview of CMIP5 and the experiment design. *Bull. Am. Meteorol. Soc.* **93**, 485–498 (2012).
 58. Van den Hurk, B. et al. LS3MIP (v1. 0) contribution to CMIP6: the land surface, snow and soil moisture model intercomparison project—aims, setup and expected outcome. *Geosci. Model. Dev.* **9**, 2809–2832 (2016).
 59. Zhao, M., Liu, Y. & Konings, A. G. Evapotranspiration frequently increases during droughts. *Nat. Clim. Change* **12**, 1024–1030 (2022).
 60. Wang, Z., Zhan, C., Ning, L. & Guo, H. Evaluation of global terrestrial evapotranspiration in CMIP6 models. *Theor. Appl. Clim.* **143**, 521–531 (2021).
 61. Dong, J., Lei, F. & Crow, W. T. Land transpiration–evaporation partitioning errors responsible for modeled summertime warm bias in the central United States. *Nat. Commun.* **13**, 336 (2022).
 62. Zhang, T. Influence of the seasonal snow cover on the ground thermal regime: an overview. *Rev. Geophys.* **43**, 1–23 (2005).
 63. Chang, X., Jin, H., Zhang, Y. & Sun, H. Study of seasonal snow cover influencing the ground thermal regime on western flank of Da Xing'anling Mountains, northeastern China. *Sci. Cold Arid Reg.* **7**, 666–674 (2015).
 64. Zhang, T. et al. Spatial and temporal variability in active layer thickness over the Russian Arctic drainage basin. *J. Geophys. Res. Atmos.* **110**, 1–14 (2005).
 65. Karjalainen, O., Luoto, M., Aalto, J. & Hjort, J. New insights into the environmental factors controlling the ground thermal regime across the Northern Hemisphere: a comparison between permafrost and non-permafrost areas. *Cryosphere* **13**, 693–707 (2019).
 66. Decker, K., Wang, D., Waite, C. & Scherbatskoy, T. Snow removal and ambient air temperature effects on forest soil temperatures in northern Vermont. *Soil Sci. Soc. Am. J.* **67**, 1234–1242 (2003).
 67. Niu, G.-Y. & Yang, Z.-L. Effects of frozen soil on snowmelt runoff and soil water storage at a continental scale. *J. Hydrometeorol.* **7**, 937–952 (2006).
 68. Decharme, B. et al. Impacts of snow and organic soils parameterization on northern Eurasian soil temperature profiles simulated by the ISBA land surface model. *Cryosphere* **10**, 853–877 (2016).
 69. Tokarska, K. B. et al. Past warming trend constrains future warming in CMIP6 models. *Sci. Adv.* **6**, eaaz9549 (2020).
 70. Gelaro, R. et al. The modern-era retrospective analysis for research and applications, version 2 (MERRA-2). *J. Clim.* **30**, 5419–5454 (2017).
 71. Hersbach, H. et al. The ERA5 global reanalysis. *Q. J. R. Meteorol. Soc.* **146**, 1999–2049 (2020).
 72. Billesbach, D. P. & Arkebauer, T. J. First long-term, direct measurements of evapotranspiration and surface water balance in the Nebraska SandHills. *Agric. Meteorol.* **156**, 104–110 (2012).

Acknowledgements

This study was funded by the National Natural Science Foundation of China (42275028) and the Sino-German Cooperation Group Program (GZ1447).

Author contributions

Yumeng Qiao, Guojie Wang, Daniel Fiffi Tawia Hagan: conceptualization; Yumeng Qiao, Daniel Fiffi Tawia Hagan, Shijie Li: data curation; Yumeng Qiao, Guojie Wang, Daniel Fiffi Tawia Hagan: formal analysis; Yumeng Qiao, Liangzhi Chene, Juha Aalto: methodology; Guojie Wang: funding acquisition; Supervision; Yumeng Qiao, Daniel Fiffi Tawia Hagan: visualization; Yumeng Qiao, Daniel Fiffi Tawia Hagan, Kenny Thiam Choy Lim Kam Sian: writing—original draft; Yumeng Qiao, Liangzhi Chen, Juha Aalto, Shijie Li, Xiao Zou, Jiao Lu: writing—review & editing.

Competing interests

The authors declare no competing interests.

Additional information

Supplementary information The online version contains supplementary material available at <https://doi.org/10.1038/s41612-024-00588-3>.

Correspondence and requests for materials should be addressed to Daniel Fiffi Tawia Hagan.

Reprints and permissions information is available at <http://www.nature.com/reprints>

Publisher's note Springer Nature remains neutral with regard to jurisdictional claims in published maps and institutional affiliations.

Open Access This article is licensed under a Creative Commons Attribution 4.0 International License, which permits use, sharing, adaptation, distribution and reproduction in any medium or format, as long as you give appropriate credit to the original author(s) and the source, provide a link to the Creative Commons licence, and indicate if changes were made. The images or other third party material in this article are included in the article's Creative Commons licence, unless indicated otherwise in a credit line to the material. If material is not included in the article's Creative Commons licence and your intended use is not permitted by statutory regulation or exceeds the permitted use, you will need to obtain permission directly from the copyright holder. To view a copy of this licence, visit <http://creativecommons.org/licenses/by/4.0/>.

© The Author(s) 2024, last corrected publication 2024